arXiv:1301.4063v1 [physics.optics] 17 Jan 2013

Three-dimensional orientation measurement of a single fluorescent nanoemitter by polarization analysis

Clotilde Lethiec[1,2], **Julien Laverdant**[1,2,3], **Henri Vallon**[1,2], **Clémentine Javaux**[4], **Benoît Dubertret**[4], **Catherine Schwob**[1,2], **Laurent Coolen**[1,2], **Agnès Maître**[1,2]

[1] *Université Pierre et Marie Curie-Paris 6, UMR 7588, INSP, 4 place Jussieu, Paris cedex 05, France*
[2] *CNRS, UMR 7588, INSP, 4 place Jussieu, Paris cedex 05, France*
[3] *Laboratoire PMCN, Université de Lyon, Université Lyon-1, UMR CNRS 5586, 69622 Villeurbanne, France*
[4] *LPEM, ESPCI/CNRS/UPMC UMR 8213, 10, Rue Vauquelin, 75005 Paris, France.*
agnes.maitre@insp.jussieu.fr

Abstract: We demonstrate theoretically and experimentally that the three-dimensional orientation of a single fluorescent nano-emitter can be obtained by polarization analysis of the emitted light (while excitation polarization analysis provides only the in-plane orientation). We point out that, in order to relate the polarization data to the orientation angles, a proper theoretical description of the experiment must be performed, including the objective numerical aperture, the 1D or 2D nature of the emitting dipole and the presence of an interface near the emitter. We develop a model covering most experimentally relevant microscopy situations and provide analytical relations which can be readily used for orientation measurements. We perform experimental orientation measurements on high-quality core-shell CdSe/CdS nanocrystals, for which we evidence a 2D emission dipole. Finally, we show that polarization analysis can provide orientation measurement even for a 2D dipole in the vicinity of a gold film, while in this case the well-established defocused microscopy is not appropriate.

© 2013 Optical Society of America

References

1. T. Ha, Th. Enderle, D. S. Chemla, P. R. Selvin and S. Weiss, ”Single molecule dynamics studied by polarization modulation”, Phys. Rev. Lett. 77, 3979 (1996),
2. E. Betzig and J. Chichester, ”Single molecules observed by near-field scanning optical microscopy”, Science 262, 1422 (1993),
3. W. Trabesinger, A. Renn, B. Hecht, U. P. Wild, A. Montali, P. Smith and C. Weder, ”Single-molecule imaging revealing the deformation-induced formation of a molecular polymer blend”, J. Phys. Chem. B 104, 5221 (2000),
4. J. N. Forkey, M. E. Quinlan, M. A. Shaw, J. E. T. Corrie and Y. E. Goldman, ”Three-dimensional structural dynamics of myosin V by single-molecule fluorescence polarization”, Nature 422, 399 (2003),
5. Erdal Toprak, Joerg Enderlein, Sheyum Syed, Sean A. McKinney, Rolfe G. Petschek, Taekjip Ha, Yale E. Goldman and Paul R. Selvin, ”Defocused orientation and position imaging (DOPI) of myosin V”, Proc. Nat. Ac. Sc. 103, 6495 (2006),
6. X. Brokmann, M.-V. Ehrensperger, J.-P. Hermier, A. Triller and M. Dahan, ”Orientational imaging and tracking of single CdSe nanocrystals by defocused microscopy”, Chem. Phys. Lett. 406, 210 (2005),
7. J. J. Macklin, J. K. Trautman, T. D. Harris and L. E. Brus, ”Imaging and time-resolved spectroscopy of single molecules at an interface”, Science 272, 255 (1996),

8. Céline Vion, Piernicola Spinicelli, Laurent Coolen, Carlos Barthou, Jean-Marc Frigerio, Jean-Pierre Hermier and Agnès Maître, ”Controlled modification of Single colloidal CdSe/ZnS quantum dots fluorescence through interactions with gold surface plasmons”, Opt. Express 18, 7440 (2010),
9. P. Bharadwaj, B. Deutsch, and L. Novotny , ”Optical Antennas”, Adv. Opt. Photon. 1, 438 (2009),
10. T. Ha, T. A. Laurence, D. S. Chemla and S. Weiss, ”Polarization spectroscopy of single fluorescent molecules”, J. Phys. Chem. B 103, 6839 (1999),
11. F. Güttler, M. Croci, A. Renn and U. P. Wild, ”Single molecule polarization spectroscopy : pentacene in p-terphenyl”, Chem. Phys. 211, 421 (1996),
12. M. A. Lieb and A. J. Meixner, ”A high numerical aperture parabolic mirror as imaging device for confocal microscopy”, Opt. Express 8, 458 (2001),
13. L. Novotny, M.R. Beversluis, K. S. Youngworth and T. G. Brown, ”Longitudinal field modes probed by single molecules”, Phys. Rev. Lett. 86, 5251 (2001),
14. B. Sick, B. Hecht and L. Novotny, ”Orientational imaging of single molecules by annular illumination”, Phys. Rev. Lett. 85, 4482 (2000),
15. R. M. Dickson, D. J. Norris and W. E. Moerner, ”Simultaneous imaging of individual molecules aligned both parallel and perpendicular to the optic axis”, Phys. Rev. Lett. 81, 5322 (1998),
16. R. Pariser, ”Theory of the electronic spectra and structure of the polyacenes and of alternant hydrocarbons”, J. Chem. Phys. 24, 250 (1956),
17. A. I. Chizhik, A. M. Chizhik, D. Khoptyar, S. Bär and A. J. Meixner, ”Excitation isotropy of single CdSe/ZnS nanocrystals”, Nano Lett. 11, 1131 (2011),
18. S. A. Empedocles and . Neuhauser and M. G. Bawendi, ”Three-dimensional orientation measurements of symmetric single chromophores using polarization microscopy”, Nature 399, 126 (1999),
19. I. Chung, K. T. Shimizu and M. G. Bawendi, ”Room temperature measurements of the 3D orientation of single CdSe quantum dots using polarization microscopy”, Proc. Nat. Ac. Sci. 100, 405 (2003),
20. X. Brokmann, L. Coolen, J-P Hermier and M. Dahan, ” Emission properties of single CdSe/ZnS quantum dots close to a dielectric interface”, Chem. Phys. Lett. 318, 91 (2005),
21. J. Hohlbein and C. G. Hübner, ”Three-dimensional orientation determination of the emission dipoles of single molecules : the shot-noise limit”, J. Chem. Phys. 129, 094703 (2008),
22. A. P. Bartko and R. M. Dickson, ”Three-dimensional orientations of polymer-bound single molecules”, J. Phys. Chem. B 103, 3053 (1999),
23. J. Jasny and J. Sepiol, ”Single molecules observed by immersion mirror objective. A novel method of finding the orientation of a radiating dipole”, Chem. Phys. Lett. 273, 439 (1997),
24. A. P. Bartko and R. M. Dickson, ”Imaging three-dimensional single molecule orientations”, J. Phys. Chem. B 103, 11237 (1999),
25. M. Böhmer and J. Enderlein, ”Orientation imaging of single molecules by wide-field epifluorescence microscopy”, J. Opt. Soc. Am. B 20, 554 (2003),
26. J. Sepiol, J. Jasny, J. Keller and U. P. Wild, ”Single molecules observed by immersion mirror objective. The orientation of terrylene molecules via the direction of its transition dipole moment”, Chem. Phys. Lett. 273, 444 (1997),
27. D. Patra, I. Gregor and . Enderlein, ”Image analysis of defocused single-molecule images for three-dimensional molecule orientation studies”, J. Phys. Chem. A 108, 6836 (2004),
28. J. T. Fourkas, ”Rapid determination of the three-dimensional orientation of single molecules”, Opt. Lett. 26, 211 (2001),
29. W. Lukosz, ”Light emission by multipole sources in thin layers. I. Radiation patterns of electric and magnetic dipoles”, J. Opt. Soc. Am. 71, 744 (1981),
30. R. J. Epstein, F. M. Mendoza, Y. K. Kato and D. D. Awschalom, ”Anisotropic interactions of a single spin and dark-spin spectroscopy in diamond”, Nat. Phys. 1, 94 (2005),
31. Al. L. Efros, M. Rosen, M. Kuno, M. Nirmal, D. J. Norris and M. G. Bawendi, ”Band-edge exciton in quantum dots of semiconductors with a degenerate valence band : dark and bright exciton states”, Phys. Rev. B 54, 4843 (1996),
32. Benoit Mahler, Piernicola Spinicelli, Stephanie Buil, Xavier Quelin, Jean-Pierre Hermier and Benoit Dubertret, ”Towards non-blinking colloidal quantum dots”, Nature Mat. 7, 659 (2008),
33. A. Cyphersmith, K. Early, A. Maksov, J. Graham, Y. Wang and M. Barnes, ”Disentangling the role of linear transition dipole in band-edge emission from single CdSe/ZnS quantum dots : combined linear anisotropy and defocused emission pattern imaging”, Appl. Phys. Lett. 97, 121915 (2010),
34. K. T. Early, K. D. McCarthy, M. Y. Odoi, P. K. Sudeep, T. Emrick and M. D. Barnes, ”Linear dipole behavior in single CdSe-oligo(phenylene vinylene) nanostructures”, ACS Nano 3, 453 (2009),
35. D. Axelrod, ”Carbocyanine dye orientation in red cell membrane studied by microscopic fluorescence polarization”, Biophys. J. 26, 557 (1979),
36. E. Rothenberg, Y. Ebenstein, M. Kazes and U. Banin, ”Two-photon fluorescence microscopy of single semiconductor quantum rods : direct observation of highly polarized nonlinear absorption dipole”, J. Phys. Chem. B 108, 2797 (2004),

37. X. Chen, A. Nazzal, D. Goorskey, M. Xiao, Z. A. Peng and X. Peng, ”Polarization spectroscopy of single CdSe quantum rods”, Phys. Rev. B 64, 245304 (2001),
38. J. Hu, L. Li, W. Yang, L. Manna, L. Wang and A. P. Alivisatos, ”Linearly polarized emission from colloidal semiconductor quantum rods”, Science 292, 2060 (2001),
39. F. Pisanello, L. Martiradonna, G. Lemenager, P. Spinicelli, A. Fiore, L. Manna, J.-P. Hermier, R. Cingolani, E. Giacobino, M. De Vittorio and A. Bramati, ”Room temperature-dipolelike single photon source with a colloidal dot-in-rod”, Appl. Phys. Lett. 96, 033101 (2010),
40. C. Belacel, B. Habert, F. Bigourdan, F. Marquier, J-P. Hugonin, S. Michaelis de Vasconcellos, X. Lafosse, L. Coolen, C. Schwob, C. Javaux, B. Dubertret, J-J. Greffet, P. Senellart and A. Maitre, ”Controlling spontaneous emission with plasmonic optical patch antennas”, arXiv 1209.6566 (2012).
41. X. Brokmann, E. Giacobino, M. Dahan and J. P. Hermier, ”Highly efficient triggered emission of single photons by colloidal CdSe/ZnS nanocrystals”, Appl. Phys. Lett. 85, 712 (2004),

---

1. Introduction

Measuring the orientation of a single photoluminescent emitter has been a subject of interest since the first single-molecule studies [1, 2]. It is a valuable tool for understanding distortion mechanisms in polymers [3] or biological systems [4, 5]. For nano-optics and plasmonics, the orientation of an emitter can have a strong influence on its coupling to an interface [7, 6, 8] or a nanoantenna [9].

First orientation studies used a rotating polarizer placed in the excitation beam [10]. In this configuration, at the focusing point of the excitation beam, the electric-field orientation is very close to the polarizer orientation [10]. The electric field thus probes the in-plane component of the dipole, and its azimutal orientation Φ can be inferred, but the (out-of-plane) polar orientation Θ remains unknown [11]. In order to measure Θ, various sophisticated schemes have been proposed to increase the out-of-plane component of the electric field [2, 12, 13, 14, 15].

These works intrinsically probe the orientation of the absorbing dipole, which for non-resonant photoluminescence can be extremely different from the emitting dipole. Depending on their group symmetry, molecules can have orthogonal excited and emitting dipoles [16]. As for colloidal semiconductor nanocrystals, while they show little dependence on the excitation polarization [17], probably because of their dense continuum of absorption levels, their emission is usually described as a sum of two incoherent orthogonal dipoles (referred to as ”two-dimensional (2D) dipole”) [18, 19, 20]. The orientation of such a nanocrystal can thus only be obtained from its emission properties, as its excitation properties are isotropic. Various methods have been suggested to determine the orientation Θ of an emitting dipole. They rely mostly (except [7] which uses relative lifetime differences) on probing the emission diagram by decomposing the different emission directions with an annular separating plate [21] or taking advantage of standard [15] or tailored aberrations [22]. In the latter category, a successful method has been defocused imaging [23, 24, 6, 25, 26, 27, 5], which offers the most convenient implementation. Possibly by analogy with the idea that the out-of-plane component of the *excitation* dipole cannot be probed by polarization analysis, for the *emission* dipole very little studies have considered polarization analysis for orientation measurements [28, 18].

In this paper, we show that the three-dimensional orientation (Θ,Φ) of a nano-emitter can be obtained by analyzing its emission polarization, for both 1D and 2D dipoles, provided that the objective numerical aperture is sufficient and that a proper theoretical analysis is performed. We insist that the emitter optical environment (such as proximity to an interface) must be taken into account. We provide an analytical model which can be used to interpret the data and extract (Θ,Φ) in a wide range of realistic experimental conditions. We demonstrate this experimentally by measuring the orientation of high-quality thick-shell CdSe/CdS nanocrystals with 2D-dipolar emission, including in proximity to a gold film, a situation for which the more standard defocused imaging cannot be used.

In the first section, we present the elements of our theoretical model. In a second section, we detail the difference between 1D and 2D dipoles and show experimentally that our CdSe/CdS nanocrystals are 2D dipoles. In the third section, we develop the results of the theoretical model and show that the orientation can be extracted from polarization data. We implement this experimentally in the fourth section and measure the orientation of various nanocrystals. In the last section, we consider the case of a nanocrystal near a metallic film, and show that the orientation can be obtained from polarization analysis but not from defocused imaging.

2. Theoretical framework

In this section we develop the theoretical modelization used in this study. The simulated situation is schematized on Fig.1(a) and (b) : the emission of a dipole is collected by an objective and analyzed by a rotating polarizer. The polarizer orientation angle α is continuously rotated. The principle of the measurement is to extract, from the detected intensity $I(\alpha)$, the azimuth angle Φ and the polar angle Θ of the emitting dipole.

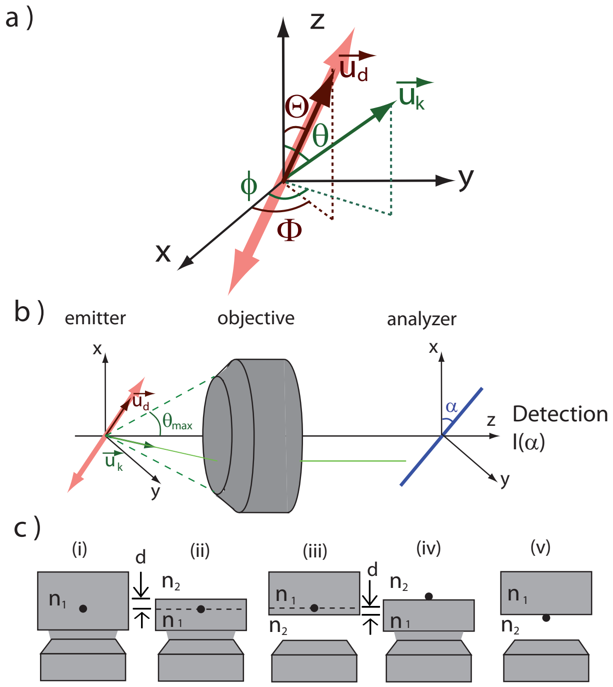

Figure 1. a)Schematic of a normalized dipole $\vec{u}_d$ with in-plane angle Φ and off-axis angle Θ and a normalized wave vector $\vec{u}_k$ with in-plane angle ϕ and off-axis angle θ. b)Schematic of the simulated situation: the dipole described above, a microscope objective, and a polarizer with in-plane angle α. c) The five cases correponding to different experimental conditions, numbered from (i) to (v).

The far-field component of the electric field emitted by a linear dipole (1D-dipole) into a direction (θ, ϕ) can be expressed as :

$$\vec{E}(\theta,\phi) = (\vec{u}_k \wedge \vec{u}_d \wedge \vec{u}_k) \tag{1}$$

where

$$\vec{u}_d = \begin{pmatrix} \sin\Theta\cos\Phi \\ \sin\Theta\sin\Phi \\ \cos\Theta \end{pmatrix} \text{ and } \vec{u}_k = \begin{pmatrix} \sin\theta\cos\phi \\ \sin\theta\sin\phi \\ \cos\theta \end{pmatrix} \tag{2}$$

are the unit vectors corresponding respectively to the dipole orientation and to the considered emission $\vec{k}$-vector direction. In this expression, $\vec{E}$ is a normalized field which does not include the $1/r^2$ and λ dependances, which are not necessary to the present study.

Equation 1 expresses the emission of a dipole in a homogeneous dielectric environment. However, in many experimental observation conditions, the dipole is in the vicinity of an optical interface, which modifies the emission diagram and polarization [29]. We describe here five relevant experimental conditions, as presented in Fig.1(c). Aside from the case of a homogeneous medium (i), we consider :

- (ii) a sample with emitters deposited on a planar substrate of index n_1 and protected from oxidation by a polymer layer of thickness d of same index, observed with an immersion objective, the upper medium (most likely air) being of index n_2,
- (iii) the same sample observed with an air objective,
- (iv) a sample with emitters on a planar surface without any protecting layer, observed with an immersion objective,
- (v) the same sample observed with an air objective.

The description of these situations requires to decompose the field $\vec{E}$ into its s and p components. The emission in a homogeneous medium (eq. 1) can be written :

$$\vec{E} = E_s\vec{u}_s + E_p\vec{u}_p \tag{3}$$

with the unit vectors:

$$\vec{u}_s = \begin{pmatrix} \sin\phi \\ -\cos\phi \\ 0 \end{pmatrix} \text{ and } \vec{u}_p = \begin{pmatrix} \cos\theta\cos\phi \\ \cos\theta\sin\phi \\ -\sin\theta \end{pmatrix} \tag{4}$$

and

$$E_s = \sin\Theta\sin(\phi-\Phi) \qquad \text{and} \qquad E_p = E_{p1} + E_{p2} \tag{5}$$

with

$$E_{p1} = -\cos\Theta\sin\theta \quad \text{and} \quad E_{p2} = \sin\Theta\cos\theta\cos(\Phi-\phi) \tag{6}$$

As for situations (ii) to (v), the presence of a near interface can be described most generally by introducing the functions $f_s(\theta)$, $f_{p1}(\theta)$ and $f_{p2}(\theta)$:

$$\vec{E} = E_s(\theta,\phi)f_s(\theta)\vec{u}_s + [E_{p1}(\theta,\phi)f_{p1}(\theta) + E_{p2}(\theta,\phi)f_{p2}(\theta)]\vec{u}_p \tag{7}$$

with an appropriate definition of these functions for each situation, depending whether it involves reflection or transmission of the emitted field [29] :

	$f_s(\theta) =$	$f_{p1}(\theta) =$	$f_{p2}(\theta) =$
(i)	1	1	1
(ii)	$1+r_s^{12}e^{i\Delta}$	$1+r_p^{12}e^{i\Delta}$	$1-r_p^{12}e^{i\Delta}$
(iii)	t_s^{12}	t_p^{12}	t_p^{12}
(iv)	t_s^{21}	t_p^{21}	t_p^{21}
(v)	$1+r_s^{21}$	$1+r_p^{21}$	$1-r_p^{21}e^{i\Delta}$

with $\Delta(\theta) = 4\pi n_1 d\cos(\theta)/\lambda$ and the Fresnel reflection and transmission coefficients :

$$r_s^{12} = \frac{n_1\cos\theta - n_2\cos\theta'}{n_1\cos\theta + n_2\cos\theta'} \tag{8}$$

$$r_p^{12} = \frac{n_2\cos\theta - n_1\cos\theta'}{n_1\cos\theta' + n_2\cos\theta} \tag{9}$$

$$t_s^{12} = \frac{2n_1\cos\theta}{n_1\cos\theta + n_2\cos\theta'} \tag{10}$$

$$t_p^{12} = \frac{2n_1\cos\theta}{n_1\cos\theta' + n_2\cos\theta} \tag{11}$$

with $n_1\sin\theta = n_2\sin\theta'$.

We now describe the collection of the emitted field by the microscope objective. The emitter is placed at the objective focal plane so that the electric field, emitted by the dipole into a direction (θ,ϕ), becomes after passage through the objective (neglecting aberrations) :

$$\vec{E}' = E_s(\theta,\phi)f_s(\theta)\vec{v}_s + [E_{p1}(\theta,\phi)f_{p1}(\theta) + E_{p2}(\theta,\phi)f_{p2}(\theta)]\vec{v}_p \tag{12}$$

with the new unit vectors :

$$\vec{v}_s = \vec{u}_s \qquad \text{and} \qquad \vec{v}_p = \begin{pmatrix} \cos\phi \\ \sin\phi \\ 0 \end{pmatrix} \tag{13}$$

The objective collects the beams for all values of ϕ between 0 and 2π and for θ between 0 and θ_{max}. The maximum collection angle θ_{max} is related to the objective numerical aperture NA by $\theta_{max} = \mathrm{asin}(NA/n_1)$ for situations (i) to (iii) and $\theta_{max} = \mathrm{asin}(NA/n_2)$ for situations (iv) and (v).

Finally, a polarizer is set along a unit vector $\vec{u}_\alpha$ at an angle α from the x-axis, so that the normalized intensity detected after the polarizer is :

$$I(\alpha) = \int_{\theta=0}^{\theta_{max}} \int_{\phi=0}^{2\pi} |\vec{E}'.\vec{u}_\alpha|^2 \sin\theta \, d\theta \, d\phi \tag{14}$$

3. Determination of the emitting dipole dimension

We have treated up to now the case of a standard linear dipole, which will be called hereafter ”1D dipole”. However, in many cases the emission originates from two degenerate states of orthogonal orientations. The emission is then an incoherent sum of two orthogonal 1D dipoles and is referred to as ”2D dipole”. Such a situation has been reported for some molecules such as benzene [16], for some nitrogen-vacancy centers [30] and for CdSe/ZnS colloidal nanocrystals at low [18] and room temperature [19, 20]. The latter observation has been related to theoretical calculations of the emitting state fine structure [31] predicting that the lowest allowed transition was twofold degenerate.

In this section, we characterize experimentally the 1D or 2D nature of the emitters considered in this paper. In order to measure the dimension of a dipole, we use the experimental setup suggested by Chung et al. [19] (fig.2 a)) which images simultaneously the x and y-polarized emission of the same emitters on two charge-coupled-device (CCD) cameras situated after a polarizing beamsplitter. For practical reasons, the polarizing beamsplitter cube in our experiment had to be placed between the eyepiece and the CCD detector, where the optical beam is collimated, so that our theory is valid. The sample is prepared in configuration (ii) : a glass sample covered by d = 50 nm of polymer of index n_1 = 1.5, with air index n_2 = 1, and a numerical aperture 1.4.

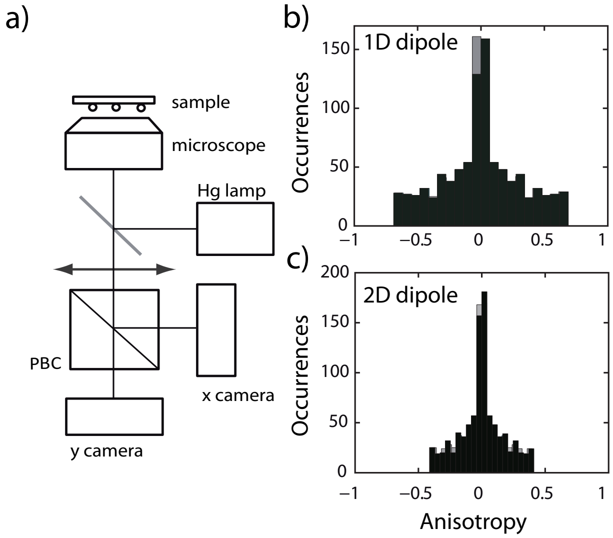

Figure 2. (a): Schematic of the setup. A polarizing beamsplitter cube (PBC) is placed in front of two CCD-cameras (directions x and y). b) and c) : Distribution of the anisotropy $A = (I_x - I_y)/(I_x + I_y)$ simulated for randomly-oriented 1D dipoles and 2D-dipoles. Calculations performed for situation (ii) with n_1 = 1.5, n_2 = 1, d = 50 nm, λ = 620 (dark grey) and 565 nm (light grey) and a 1.4 numerical aperture.

It is then possible to image many emitter and for each emitter to measure the intensities I_x and I_y on the two cameras and define a polarization anisotropy A :

$$A = \frac{I_x - I_y}{I_x + I_y} \tag{15}$$

On the other hand, A can be calculated, for a given dipole with an orientation (Θ,Φ), from equation (14) because :

$$I_x = I(\alpha = 0) \tag{16}$$

$$I_y = I(\alpha = \frac{\pi}{2}) \tag{17}$$

We assume a collection of emitters with random orientations isotropically distributed and plot a histogram of the calculated anisotropies, for 1D and 2D dipoles (Fig.2(b) ; we consider the two wavelengths 565 and 620 nm as they will be relevant for the experiment below). Both histograms display a peak at $A = 0$ but the extension of the wings on either side of this peak is different : for a 1D-dipole, the wings extend up to ± 0.7 while for a 2D-dipole they extend only to ± 0.4. It is thus possible, by measuring the anisotropy of randomly oriented emitters and plotting a histogram of these anisotropies, to discriminate whether this type of emitters is 1D or 2D. Let us note that this calculation is performed for situation (ii) with the parameters indicated above : in a different configuration, the results would be quantitatively slightly different but the qualitative difference between 1D and 2D dipoles would remain.

The experimental results obtained for different types of emitters are shown on Fig.3.

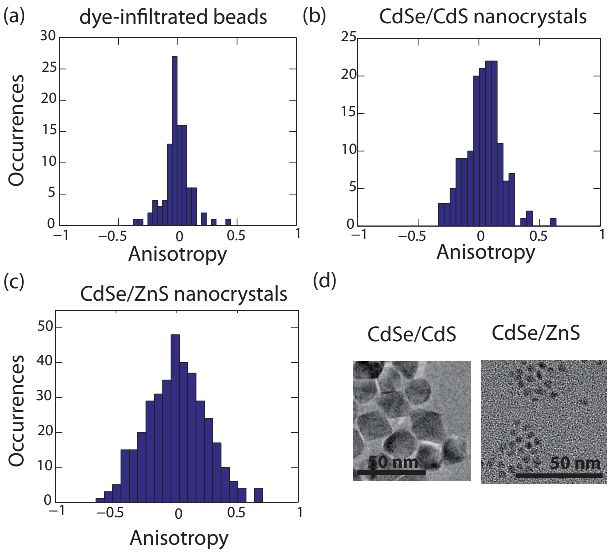

Figure 3. Distribution of the anisotropy $A = (I_y - I_x)/I_y + I_x)$ measured for 103 beads (a), 152 CdSe/CdS nanocrystals (b) and 374 CdSe/ZnS nanocrystals. (c) Experimental conditions : situation (ii), numerical aperture 1.4, textcolorred d = 50 nm of PMMA of index 1.5. (d) Transmission electron microscopy image of the CdSe/CdS and CdSe/ZnS nanocrystal samples.

Latex beads infiltrated with dye molecules (Lifetechnologies, F8763, emission peak at 600 nm) are first studied in order to validate the method. Each bead contains a large number of emitters so that the polarization anisotropy should be exactly zero for all beads. Indeed, we obtain (Fig.3(a), error bar: 0.05) a peak centered on $A = 0$, with a width 0.05 attributed to measurement uncertainties.

We then study colloidal core/shell CdSe/CdS nanocrystals (emission 620nm, core diameter 2.5 nm, total diameter 13 nm) exhibiting very good brightness and suppressed blinking [32] (fig. 3(d)). The obtained anisotropy histogram (Fig.3(b), error bar: 0.05) presents a peak on zero and the extension of the curve reaches ±0.4. This experimental curve is in satisfying agreement with the theoretical curve of Fig.2(c), taking into account a slight broadening of the central peak due to the 0.05 uncertainty on A. This demonstrates that these nanocrystals are 2D dipoles. If they were 1D dipoles, their anistropy histogram would extend up to ±0.7.

Finally, we consider core/shell CdSe/ZnS nanocrystals (QDots, Invitrogen, emission 565nm) (fig. 3(d)). For such nanocrystals, Empedocles et al. have reported a 2D dipole behavior [18]. The experimental histogram obtained for these nanocrystals is plotted in Fig.3(c). The error bar is here more important (0.1) because the emission intensity is lower for these emitters. The curve presents a peak at zero and wings extending to ±0.5. The agreement with the theoretical histogram for 2D dipoles is not very good, possibly because of a mixture of 1D and 2D dipolar emission as suggested in [33] and [34].

4. Theoretical results

We now return to the main point of this paper which is the determination of the orientation of a single emitter. We elaborate here on the theory of section I and show that the emitting dipole orientation can be extracted from a polarization analysis.

We distinguish between 1D and 2D dipoles as the importance of this difference was pointed out in the previous section. The orientation (Θ,Φ) of a 1D-dipole is defined as in section I. For a 2D dipole, (Θ,Φ) will refer to the orientation of the emitter dark axis [18] : the axis normal to the plane containing the two emitting dipoles. Since the two dipoles are incoherent, the intensity emitted by a 2D dipole of dark-axis orientation (Θ,Φ) can be calculated as a sum of the intensities emitted by two 1D dipoles of orientations ($\pi/2-\Theta,\Phi$) and ($\pi/2,\Phi+\pi/2$).

After some manipulation, the measured intensity as a function of a rotating polarizer angle α (eq. 14) can be written as :

$$I_{1D}(\alpha) = I_{min} + (I_{max} - I_{min})\cos^2(\Phi-\alpha) \tag{18}$$

$$I_{2D}(\alpha) = I_{max} + (I_{min} - I_{max})\cos^2(\Phi-\alpha) \tag{19}$$

This expression shows that the emitted intensity is partially polarized for both 1D and 2D dipoles, with a Malus component in $\cos^2(\Phi-\alpha)$ from which the emitter in-plane orientation Φ can be straightforwardly extracted, as was done in many papers. Let us stress out however that Φ is obtained as the polarizer angle which *maximizes* the detected intensity for a 1D dipole, but as the angle which *minimizes* the intensity for a 2D dipole (because Φ is the orientation of the "dark axis").

We now express the maximum intensity I_{max} and minimum intensity I_{min} and show that their knowledge can lead to Θ. For a 1D-dipole:

$$I_{min} = A\sin^2\Theta + B\cos^2\Theta \tag{20}$$

$$I_{max} - I_{min} = C\sin^2\Theta \tag{21}$$

and for a 2D-dipole:

$$I_{min} = A + B + (A - B + C)\cos^2\Theta \tag{22}$$

$$I_{max} - I_{min} = C\sin^2\Theta \tag{23}$$

with, for both 1D and 2D dipoles, the constants :

$$A = \int_{\theta=0}^{\theta_{max}} \frac{\pi}{4} |f_s(\theta) - \cos\theta f'_p(\theta)|^2 \sin\theta d\theta \tag{24}$$

$$B = \int_{\theta=0}^{\theta_{max}} \pi |f_p(\theta)|^2 \sin^3\theta d\theta \tag{25}$$

$$C = \int_{\theta=0}^{\theta_{max}} \frac{\pi}{2} |\cos\theta f'_p(\theta) + f_s(\theta)|^2 \sin\theta d\theta \tag{26}$$

From an experimental perspective, the measured I_{max} and I_{min} are both proportionnal to the total emitted intensity (here normalized in the calculation), which is not known experimentally so that a normalized quantity must be extracted. Usually one defines the degree of linear polarization of the emission as:

$$\delta(\Theta) = \frac{I_{max} - I_{min}}{I_{max} + I_{min}} \tag{27}$$

Including equations (20) to (23) in equations (18) and (19), one obtains, for a 1D-dipole and 2D-dipole respectively :

$$\delta(\Theta)_{1D} = \frac{C\sin^2\Theta}{(2A - 2B + C)\sin^2\Theta + 2B} \tag{28}$$

$$\delta(\Theta)_{2D} = \frac{C\sin^2\Theta}{-(2A - 2B + C)\sin^2\Theta + 4A + 2C} \tag{29}$$

In the case of a vertical dipole ($\Theta = 0$), the emission is fully unpolarized for both 1D and 2D dipoles ($\delta = 0$), as expected given that the system then has cylindrical symmetry. As the angle Θ is increased, the emission becomes more polarized and, for $\Theta = \pi/2$, δ reaches a maximum value of $C/(2A + C)$ for a 1D-dipole and $C/(2A + 2B + C)$ for a 2D-dipole, which is always smaller than unity : the emission in never strictly fully polarized.

These equations show that, for both 1D and 2D dipoles, it is possible to extract the out-of-plane orientation Θ from the measured degree of polarization δ. This requires the knowledge of the coefficients A, B and C, which can be calculated theoretically for a given situation and depend on the sample configuration (presence of an interface) through the functions f_s, f_{p1} and f_{p2}, and on the objective numerical aperture through θ_{max}.

Let us discuss briefly the difference between excitation and emission polarization analysis. A typical excitation polarization analysis setup will include a rotating polarizer of angle α_{exc} on the path of the excitation beam, and measure the emitted intensity $I(\alpha_{exc})$. It was shown in ref.[10] that the orientation of the exciting electric field $\vec{E}_{exc}$, at the position of the emitter, is very close to the orientation $\vec{u}_{\alpha,\text{exc}}$ of the excitation polarizer, even when taking into account emitter positioning imperfections and a high objective numerical aperture. The measured quantity is then, for a 1D dipole :

$$\begin{aligned} I(\alpha) &\propto |\vec{d}.\vec{E}_{exc}|^2 \\ &\propto I_0 |\vec{u}_d.\vec{u}_\alpha|^2 = I_0 \cos^2(\Phi - \alpha_{exc}) \sin^2\Theta \end{aligned} \tag{30}$$

In this case, as pointed out since early work on single-molecule orientation [7, 1], the in-plane angle Φ can be obtained as the angle α_{exc} which maximizes $I(\alpha_{exc})$ but the out-of-plane angle Θ cannot be obtained because the value I_0 is not known. It is clear, by comparison of expressions (18) and (30), that the polarization analysis in excitation and emission are two very different situations.

We now discuss the calculated correspondance between Θ and δ and analyze its physical meaning.

We start with an emitter in a homogeneous medium (situation (i)). The values of A, B and C can then be calculated analytically [35] and in the limit of high numerical aperture ($\theta_{\text{max}} = \pi/2$) we find for a 1D dipole the simple expression :

$$\delta_{\text{high NA}}(\Theta) = \frac{7}{8}\sin^2\Theta \tag{31}$$

so that δ ranges from 0 to 0.875. On the other hand, for a 1D dipole in the limit of a low numerical aperture, a second-order development in θ_{max} leads to :

$$\delta_{\text{low NA}}(\Theta) = \frac{\sin^2\Theta}{(1-\frac{\theta_{\text{max}}^2}{2})\sin^2\Theta + \frac{\theta_{\text{max}}^2}{2}} \tag{32}$$

In this case, the maximum value of δ is 1. The case of $\theta_{max} \sim 0$ (very low numerical aperture) is interesting as it corresponds to probing a single direction of emission. Our calculations show that, for $\theta_{max} \sim 0$, δ is unity for any Θ, as expected since the emission of a 1D dipole into a specific direction is always polarized (the case $\Theta = 0$ is an exception : it gives $\delta = 0$, but is actually not measurable because no light can be detected for this orientation : a 1D dipole never emits into the direction of its axis). This means that a very low numerical aperture is not an appropriate condition for measuring the orientation of an emitter by polarization analysis : the angle Θ cannot be deduced from the value of δ as it is always unity. As the numerical aperture is increased, the objective collects the emission into different directions, each direction having a specific polarization, so that the collected beam is a summation of different polarizations and has a lower degree of polarization. It is this summation which allows the measurement of Θ from the polarization properties.

As for a 2D dipole in a homogeneous medium, it can also be calculated analytically that for a high numerical aperture ($\theta_{\text{max}} = \pi/2$) :

$$\delta_{\text{high NA}}(\Theta) = \frac{7}{16}\sin^2\Theta \tag{33}$$

which is half the degree of polarization in the 1D case (similar trends are also observed for situations (ii) and (iv) in fig. 4(a) and (b)). It is not surprising that a 2D dipole, being a sum of two incoherent dipoles, emits with a lower degree of polarization. In the limit of low numerical aperture,

$$\delta_{\text{low NA}}(\Theta) = \frac{\sin^2\Theta}{(\frac{\theta_{\text{max}}^2}{2} - 1)\sin^2\Theta + 2} \tag{34}$$

We note here that, for $\theta_{\text{max}} \sim 0$, which corresponds to probing a single direction of emission, δ is not always unity, unlike the case of a 1D dipole. This is explained by the fact that, even when probing a single emission direction, the emission is not necessarily polarized as it is a sum of the emissions of two incoherent dipoles with different polarizations.

We now turn to the cases where the emitter is near an interface. We have introduced in section I several standard experimental conditions. We plot in fig. 4 the relation between Θ and δ for the following parameters : $n_1 = 1.5$, $n_2 = 1$, d = 50 nm, λ = 620 nm. We consider the case of a 0.7 numerical aperture for situations (i) to (v), and the case of an immersion objective with 1.4 numerical aperture for situations (i), (ii) and (v). We distinguish between 1D and 2D dipoles. The obtained curves show a similar trend, with an increase from $\delta(0) = 0$ to a maximum $\delta(\pi/2)$ which is always below 1. However, the quantitative differences between these curves are significant. For a given value of δ, depending on the experimental configuration and on the 1D or 2D nature of the dipole, the corresponding values of Θ can be different by up to 35°. It is thus possible, in all these experimental configurations, to extract Θ from δ, but only if the specificities of this configuration (numerical aperture, 1D/2D nature, index, interface etc) are properly included in the theoretical analysis.

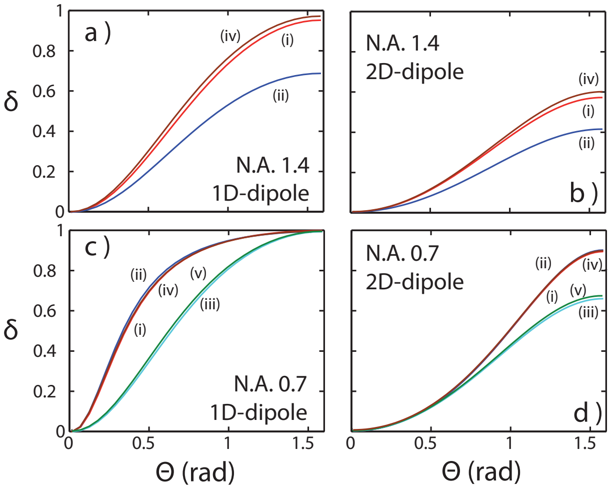

Figure 4. Theoretical value of δ a function of the angle Θ for a 1D dipole (a,c) or a 2D dipole (b,d) with numerical aperture 1.4 (a,b) or 0.7 (c,d), calculated in situations (i), (ii) and (iv) for (a,b) and situations (i) to (v) for (c,d) with the parameters n_1 = 1.5, n_2 = 1, d = 50 nm and λ = 620 nm.

Finally, let us discuss the polarization analysis in the case of nanorod emission [37, 38, 36, 39]. In these studies, the nanorods are assumed horizontally deposited ($\Theta = \pi/2$), and the degree of linear polarization δ is measured in order to probe to which extent the rod behaves as a linear dipole. Our curves show that, if the rod is a perfect 1D dipole, a value $\delta \simeq 1$ should be measured in all situations for a 0.7 numerical aperture, but, for a 1.4 numerical aperture, values of δ between 0.7 and 0.98 are calculated, depending on the situation. This must be taken into account when interpreting the experimental values of δ, which range from 0.7 to 0.9 [37, 38, 39].

5. Experimental orientation measurement

In this section, we apply these considerations to demonstrate experimental orientation measurements on CdSe/CdS nanocrystals, chosen for their brightness and photostability.

We use an inverted microscope to image a sample of CdSe/CdS nanocrystals on a glass substrate, covered by 50 nm of PMMA (measured by profilometer), with an oil-immersion objective (1.4 numerical aperture, x100). A single nanocrystal is excited by a diode laser at 450 nm (we confirm for each measurement that only a single nanocrystal is imaged by performing a standard Hanbury-Brown and Twiss measurement and showing that the nanocrystal emits single photons [41]). The photoluminescence is collected by the same objective and focused on a 100-μm pinhole in order to spatially filter the background noise. It is then recollimated, passed through a half-wave plate, separated into two arms by a polarizing beamsplitting cube and each arm is focused on a single-photon counting avalanche photodiode (see inset of fig. 5(a)). The half-wave plate is continuously rotated with an angle $\alpha/2$ and the photoluminescence intensity is measured on each photodiode. The role of the half-wave plate and polarizing cube is equivalent to a polarizer of angle α.

We plot in fig. 5(a) the intensity on one photodiode, normalized by the sum of the intensities on the two photodiodes in order to cancel the fluctuations of the total emitted intensity, due to slight emitter unstabilities. This curve is well fitted by equation (19) with 3 fitting parameters : I_{max}, $I_{min} - I_{max}$ and Φ. We find, for this nanocrystal, an in-plane angle $\Phi = 50^{o}$ and a degree of polarization δ =18% from which we deduce, given the theoretical curve of fig. 4(b) (situation (ii)), an out-of-plane angle $\Theta = 43^{o}$. We estimate the precision of our fit to $\pm$ 4 ^{o} for Φ, and $\pm$ 2 ^{o} on Θ.

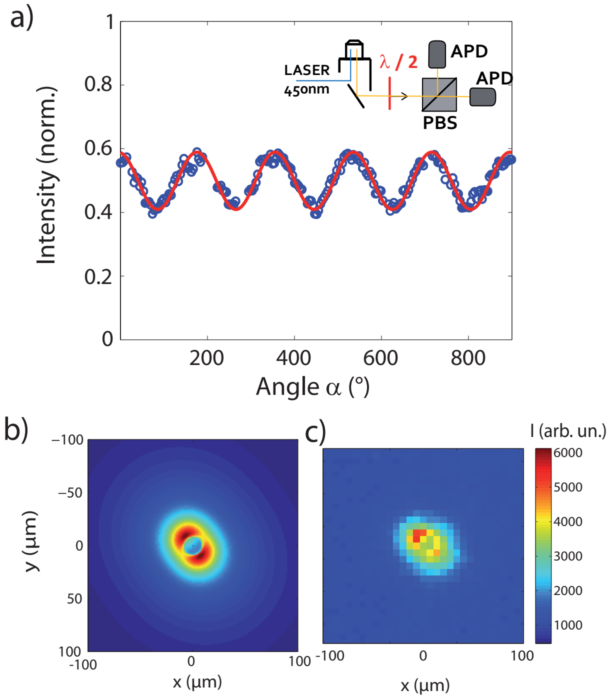

Figure 5. (a) Circles : dependance of detected intensity as a function of polarization analysis angle for a nanocrystal of CdSe/CdS at the vicinity of air/dielectric interface. This curve is normalized by the total emitted intensity in order to account for fluctuations of the total emitted intensity. The different detection efficiencies of the two paths are corrected so that the normalized curve has a mean value of 0.5. The fitted curve (solid red line) corresponds to equation (19). We deduce from the fit Θ=44° and Φ=52°. (b) Theoretical defocused image of a single 2D-dipole oriented with Θ=44° and Φ=52° (in the imaging plane, with 1 μm defocusing and x100 magnification). (c) Experimental CCD image of the nanocrystal with 1 μm defocusing.

We repeat this measurement for a collection of the CdSe/CdS nanocrystals and plot in fig.6(a) a histogram of the obtained values of δ. We find values of δ below 0.4, in agreement with our theoretical calculation (fig. 4(b), situation (ii)) that the value of δ ranges between 0 and 0.4 for a 2D dipole in this configuration. This is consistent with our previous demonstration that the CdSe/CdS nanocrystals are 2D emitters. On the other hand, we perform the same measurements for a collection of CdSe/ZnS nanocrystals (fig. 6(a)) and we find values of δ up to 0.7. These values are too high for a 2D dipole, as shown by fig. 4(b) (for the CdSe/ZnS nanocrystals of emission wavelength λ = 565 nm, the calculated curve is not shown here but very close to the case λ = 620 nm). They could be explained by a mixture of 1D and 2D dipoles as already proposed in section II, since the maximum theoretical δ is 0.7 for a 1D dipole.

We plot in fig. 6(b) a histogram of the out-of-plane angles Θ measured for the CdSe/CdS nanocrystals. We find a distribution of angles between 31 and 83 ^{o}. We did not find any nanocrystal with orientation Θ below 30^{o}. Indeed, small values of Θ are theoretically less likely : for an isotropic distribution of orientations (Θ,Φ), only 13 % of orientations show $\Theta < 30^\circ$. It is also possible that the predominance of the 40-60° orientations is due to the specific geometry of the CdSe/CdS nanocrystals. These thick-shell NCs are not spherical and display a faceted geometry (Fig. 3(d)). They tend to have a bi-pyramidal shape and they may lay on the substrate with some preferred orientation which could explain the bias we observed in the polarization measurements.

We finally compare our orientation measurement with the technique of defocused imaging. Defocusing the obtained image by moving the microscope objective by 1 μm places the emitters in the quasi far field. This allows to image the emission pattern of the emitters, which depends on its orientation, and provides their orientation. For the nanocrystal of fig. 5(a), we switch the detection channel to a CCD camera and defocus the sample by 1 μm. The obtained experimental defocused image is plotted in fig. 5(c). Figure 5(b) plots the theoretical defocused image calculated with the values of (Θ,Φ) obtained from the polarization analysis. This theoretical pattern is obtained by considering that the image $I(x,y)$ is related to the emission diagram $||\vec{E}(\theta,\phi)||^2$ (given by eq. (7)) by $x = M\delta z \tan\theta\cos\phi$ and $y = M\delta z \tan\theta \sin\phi$ where $M = 100$ is the magnification and δz is the defocusing. The experimental and theoretical images are in good agreement, showing that the result from our polarization analysis is consistent with the result from defocused imaging.

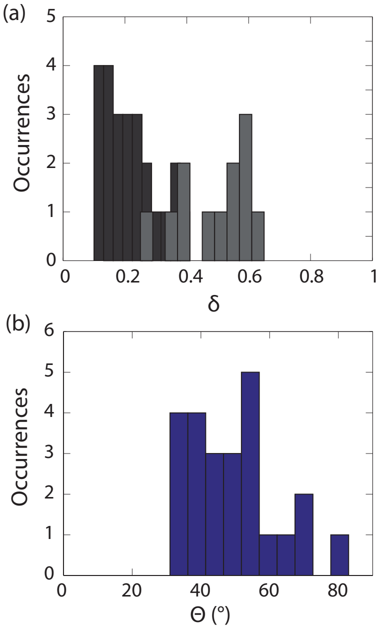

Figure 6. (a) Histogram of experimental values of δ for 24 CdSe/CdS nanocrystals (blue bars) and 13 CdSe/ZnS nanocrystals (red bars). (b) Histogram of experimental values of Θ for 24 CdSe/CdS nanocrystals.

6. Vicinity of a gold surface

Finally, we discuss in this last section the orientation measurement for an emitter in the vicinity of a gold film. This situation is of interest, for instance, in the context of coupling to surface plasmons [8] or nano antennas [40], for which the orientation is crucial. We deposit on a glass substrate 200 nm of gold, 25 nm of silica, CdSe/CdS nanocrystals, and 50 nm of PMMA (fig. 7(a)). We image this sample with an oil-immersion objective of numerical aperture 1.4.

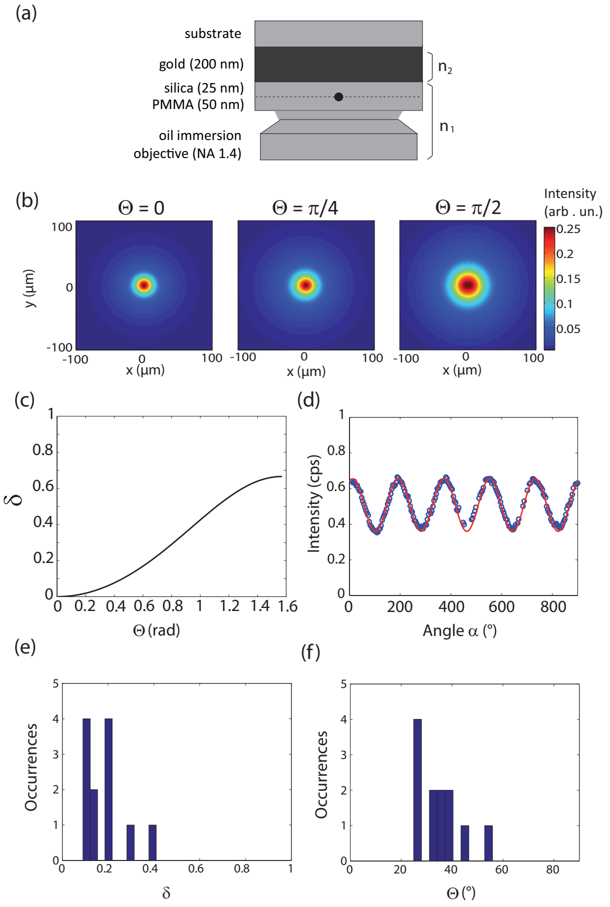

Figure 7. (a) Schematic of the experimental system. (b) Calculated defocused patterns for a 2D-dipole with (Θ=0,Φ=0), ($\Theta=\frac{\pi}{4}$,Φ=0) and ($\Theta=\frac{\pi}{2}$,Φ=0). (c) Calculated values of δ as a function of the angle Θ for a 2D-dipole (c-axis inclination). (d) Circles : dependance of the x-polarized emission intensity as a function of half-wave plate angle for a nanocrystal of CdSe/CdS at the vicinity of gold/dielectric interface, fitted (solid red line) with the equation (19). We deduce from the fit Θ=46° and Φ=69°.

Since the optical skin depth in gold is a few tens of nanometers, the 200-nm gold layer can be considered infinitely thick. We are then in the case which we labelled as situation (ii), where $n_1 = 1.5$ is the silica/PMMA index, $d = 25$ nm is the distance to the gold film, n_2 is the gold dielectric constant (obtained from ellipsometric measurements) and $\lambda = 620$ nm. We plot in fig. 7(b) the defocused image, calculated as explained in the previous section, for three different angles Θ. Apart from the total emitted intensity (which is not a useful quantity to deduce Θ as the emitted intensity can vary significantly among nanocrystals), there are very little differences between these images, so that Θ cannot be obtained. Moreover, the defocused images have rotation invariance, so that Φ cannot be known from these images either. This is an example of a situation for which defocused imaging cannot be used to measure the orientation of a dipole.

Polarization analysis, on the other hand, is appropriate in this configuration. We plot in fig. 7(c) the theoretical dependence of δ on Θ. This curve shows a sufficiently clear dependence for Θ to be determined if δ is known. We plot in fig. 7(d) the experimental polarization analysis for a CdSe/CdS nanocrystal. By fitting these data with eq. (19), we find the nanocrystal orientation : $\Phi = 69 \pm 3^o$ and $\Theta = 46 \pm 1^o$.

We make the same measurements for 12 nanocrystals on this gold-silica substrate, and plot a histogram of the measured values of δ in fig. 7(e) and of the corresponding Θ in fig. 7(f). The values of Θ are distributed between 0.1 and 0.4, in agreement with the calculations of fig. 7(c) showing that δ can range between 0 and 0.7. The corresponding orientations Θ range between 25 and 55°. These angles are consistent with the values obtained in section IV.

Conclusion

In this paper, we adressed the orientation measurement of a single photoluminescent emitter. We showed that, in contrast with excitation polarization analysis, emission polarization analysis provides both the in-plane angle Φ and the out-of-plane angle Θ. In the case of a 2D-dipole near a gold film, polarization analysis is the only appropriate method, as the more well-established defocused imaging cannot yield precise results. We developped a model of the polarization analysis experiment, and insisted on the importance of taking into account the sample geometry (presence of an interface) and the objective numerical aperture. We distinguished five different sample configurations which we believe will cover most experimental conditions, but other situations could be easily extrapolated. We showed that, in all of these situations (except in the case of an objective with very low numerical aperture), the angle Θ can be deduced from the measured degree of polarization δ, and we provided simple analytical expressions for the correspondence $\delta(\Theta)$. These expressions can lead to rather different quantitative values, depending on the experimental situation, so that the experimental situation must be carefully taken into account in the model. The 1D or 2D nature of the dipole is also an important parameter to be included in the model. We demonstrated experimentally the orientation measurement on CdSe/CdS, which we demonstrated to be 2D dipoles.

The authors would like to thank Francis Breton, Stéphane Chenot and Loïc Becerra for technical support and fabrication of the samples, Jean-Louis Fave, Michel Schott, Jean-Marc Frigerio and Paul Bénalloul for fruitful discussions. This work was funded by the Agence Nationale de la Recherche (P3N Delight) and by the Centre de Compétence NanoSciences Ile-de-France (C'Nano IdF).